ADVANCED FUNCTIONAL MATERIALS
www.afm-journal.de

Rapid Characterization of Ultrathin Layers of Chalcogenides on SiO_2/Si Substrates

*Dattatray J. Late, Bin Liu, H. S. S. Ramakrishna Matte, C. N. R. Rao, and Vinayak P. Dravid**

There has been emerging interest in exploring single-sheet 2D layered structures other than graphene to explore potentially interesting properties and phenomena. The preparation, isolation and rapid unambiguous characterization of large size ultrathin layers of MoS_2, GaS, and GaSe deposited onto SiO_2/Si substrates is reported. Optical color contrast is identified using reflection optical microscopy for layers with various thicknesses. The optical contrast of these thin layers is correlated with atomic force microscopy (AFM) and Raman spectroscopy to determine the exact thickness and to calculate number of the atomic layers present in the thin flakes and sheets. Collectively, optical microscopy, AFM, and Raman spectroscopy combined with Raman imaging data are analyzed to determine the thickness (and thus, the number of unit layers) of the MoS_2, GaS, and GaSe ultrathin flakes in a fast, non-destructive, and unambiguous manner. These findings may enable experimental access to and unambiguous determination of layered chalcogenides for scientific exploration and potential technological applications.

1. Introduction

Single-layer graphene (SLG) is the first known 2D material that can exist without a matching crystalline substrate and it can even be freely suspended. There has been intense search for other 2D materials that can be similarly be isolated from the bulk, in search for even more intriguing properties and phenomena. Indeed, Novoselov et al.[1] have suggested the possibility of extracting a single layer of other layered materials using the simple micromechanical cleavage technique. Recently one atomic layer thickness materials like SLG,[1–5] molybdenum disulfide (MoS_2),[6–11] niobium diselenide ($NbSe_2$),[12–14] and hexagonal boron nitride (h-BN)[14–15] have attracted considerable attention because of their novel optical, electrical, mechanical, and magnetic properties. These layered materials have the potential to be used in next-generation nanoelectronic devices because of their enhanced performance and unusual physics of transport and related properties.

Several methods have been reported in the literature to synthesize layered materials including micromechanical cleavage,[2] epitaxial growth,[16] chemical vapor deposition,[17] and liquid exfoliation.[18] These techniques produce not only single unit atomic layers but all types of flakes consisting of few unit layers to those approaching bulk-like materials. As a result, locating a possible single layer or a few layers within the sample is a time-consuming process. A rapid and unambiguous method for determining the number of layers of such layered specimens is essential to accelerate research and exploration of their properties. Although atomic force microscopy (AFM) is the most direct way to identify the number of layers, the method has a very slow throughput. Furthermore, an instrumental offset (caused by different interaction forces) may also exist, which can be larger than the thickness of a monolayer and data fitting is required to extract the true thickness of the layered sheets. Researchers have attempted to develop more efficient and rapid ways to identify various numbers of layers without destroying the crystal lattice. Raman spectroscopy and Raman imaging has been shown to be a potential candidate for non-destructive and rapid characterization of the number of layers.

There are a large number of technological applications in which this novel material can be employed and fast-track identification and characterization processes of single-layer and multilayers are requried.[19] Therefore, fast and unambiguous visualization techniques are striking within this promising area. Optical microscopy is a simple yet powerful, non-destructive, and efficient method to locate and identify the single-layer and few layers on a smooth and flat substrate for rapid characterization of these layered materials. The contrast between these layered materials and background is the essential factor for identification of the number of layers present in the sample and the observed contrast is small due to ultrathin nature of these layered materials (e.g., monolayer graphene has a thickness of 0.34 nm). Here, we demonstrate high efficacy preparation and rapid characterization

Dr. D. J. Late, B. Liu, Prof. V. P. Dravid
Department of Materials Science and Engineering
International Institute of Nanotechnology
Northwestern University, Evanston, IL 60208, USA
E-mail: v-dravid@northwestern.edu
H. S. S. Ramakrishna Matte, Prof. C. N. R. Rao
Chemistry and Physics of Materials Unit
CSIR Centre of Excellence in Chemistry and
International Centre for Materials Science
Jawaharlal Nehru Centre for Advanced
Scientific Research, Jakkur PO
Bangalore 560064, India

DOI: 10.1002/adfm.201102913

of layered structures utilizing corroborating and complementary characterization techniques that may prove widely applicable for unambiguous characterization of number of sheets in diverse 2D layered structures. Recently, few studies have reported on single-layer MoS_2 PL measurements,[20] Raman spectroscopy,[21] and optical contrast.[7] However, there is a notable absence of detailed investigation of synthesis of layered gallium sulfide (GaS) and gallium selenide (GaSe) as well as the effect of thickness variation of SiO_2 on optical contrast and Raman spectroscopy of these layered materials. In view of their extraordinary properties, we considered it critical to carry out a systematic optical, AFM, and Raman spectroscopy characterization.

Transition metal dichalcogenides are inorganic layered materials that exhibit a large variety and range of electronic properties such as semiconductivity, superconductivity, or charge density wave. The semiconducting dichalcogenides material MoS_2 is a promising material for electronic applications because of its high stability and transport characteristics. Hexagonal MoS_2, GaS, and GaSe have layered structures with each layer consisting of S–Mo–S, S–Ga–Ga–S, and Se–Ga–Ga–Se sheets,[22,23] respectively. The strong intralayer bonding and the weak interlayer van der Waals interaction give highly anisotropic structural, electrical, optical, and mechanical properties. The intrinsic 2D layered structures allow for relatively easy fabrication of single layers of these materials by micromechanical cleavage for testing their properties as a function of the number of layers.

The structure of MoS_2 consists of an atomic plane of Mo sandwiched between two atomic planes of S in a trigonal prismatic arrangement S–Mo–S. The bond distance of S–Mo is 1.54 Å and S–S is 3.08 Å. Therefore single-layer MoS_2 have a thickness of 0.62 nm. **Figure 1**a–c shows the crystal structure of single-layer MoS_2. In the bulk, MoS_2 is a semiconductor with a bandgap of 1.8 eV, while single-layer MoS_2 has bandgap of 1.2 eV[24] and therefore does not exhibit the complexities associated with the non-adiabatic electron–phonon coupling that is most prominent in graphene. While atoms within the layers are strongly bonded, the layers are attracted to each other by weak van der Waals forces making MoS_2 easier to cleave. This characteristic makes it compatible with the micromechanical cleavage technique to obtain single (and multi-) layers of MoS_2.[6–8,20,21] The micromechanical cleavage technique has been widely used to fabricate single-layer graphene and consists of repeatedly peeling the layered bulk material and transferring the peeled material on top of a SiO_2/Si substrate with a specific SiO_2 thickness. This technique has been proven to be an easy and relatively quick way of producing highly crystalline single-layer flakes. Also, it is relatively straightforward to identify the single-layer flakes using an optical microscope by the specific color contrast.

GaS and GaSe are equally intriguing layered semiconducting materials with indirect bandgaps of 3.05 eV and 2.1 eV, respectively, at room temperature. It is well known that hexagonal GaS and GaSe have layered structures with each layer consisting of S–Ga–Ga–S and Se–Ga–Ga–Se sheets.[22,23] Figure 1d–f shows the crystal structure of single-layer GaS/GaSe. GaS consists of a double layer of nonmetal atoms, with each sheet stacking together by the nonbonding interaction through the S atoms along the *c*-axis. It has a stable, hexagonal, double-layered structure with bond distances of 2.48 Å and 2.37 Å for the Ga–Ga and Ga–S bond lengths, respectively. There are two layers in a single GaS unit cell in which the bonding between two adjacent layers

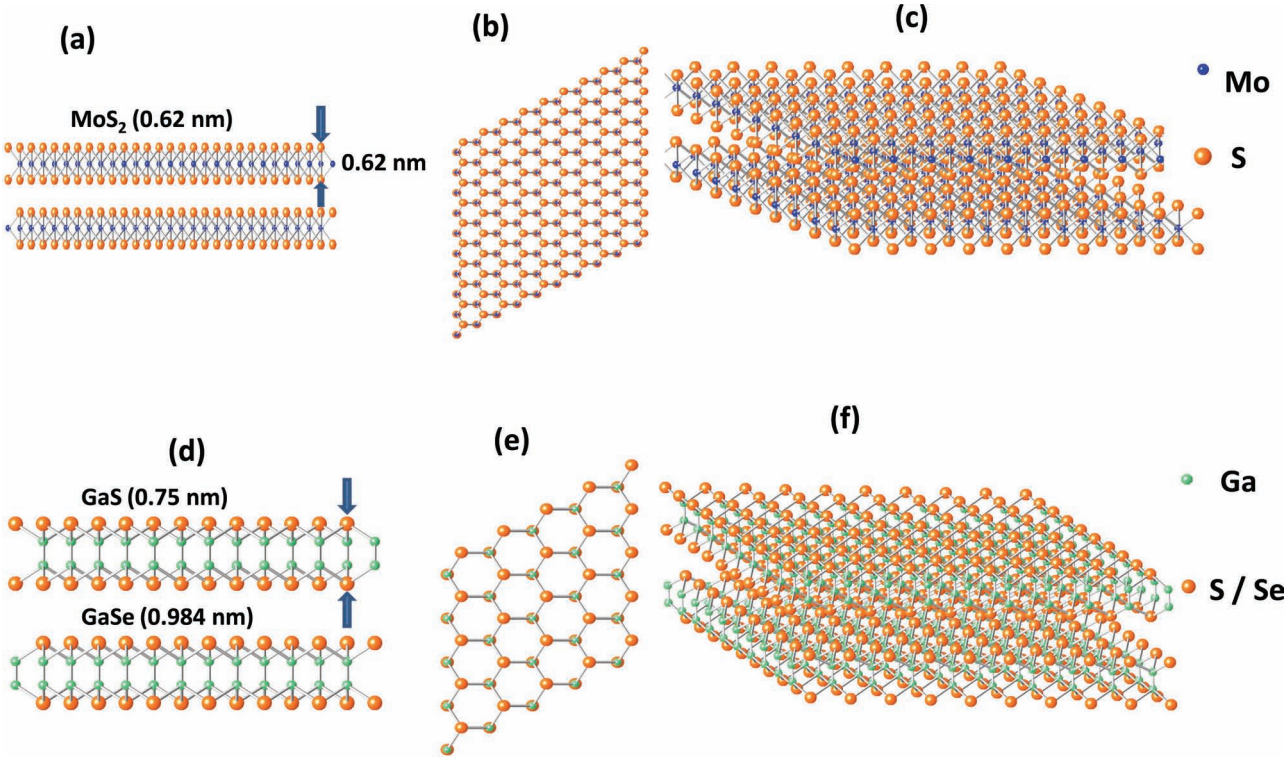

Figure 1. MoS_2 crystal structure: a) side view and b,c) top view. GaS/GaSe crystal structure: d) side view and e,f) top view.

is a van der Waals interaction and the bonding within a layer is predominantly covalent. The strong interlayer bonding and the weak interlayer van der Waals interaction gives highly anisotropic structural, electrical, optical, and mechanical properties, which have made these layered materials more attractive and promising for potential applications. The doped GaS is a promising material for the fabrication of near-blue-light emitting devices.

GaSe has hexagonal double-layered structures with bond distances of 2.45 Å and 2.46 Å for Ga–Ga and Ga–Se, respectively. Therefore, the stable form for one formula unit thickness of GaS and GaSe is about 0.75 nm (twice 0.375 nm) and 0.984 (twice 0.492 nm), respectively. There have been few reports on synthesis of nanostructured GaS such as nanowires,[25] nanotubes,[26,27] and nanowalls.[28] There are handful studies on nanostructured GaSe such as nanowires[29] and nanowalls.[28] However, there is notable absence of a detailed study of the effect of the thickness variation of SiO_2 on the contrast of these layered materials and there is only one report on MoS_2[7] at the time of this submission.

Here, we report our investigations on the synthesis of ultrathin layers of MoS_2, GaS, and GaSe using micromechanical cleavage technique on 50 nm, 300 nm, and 500 nm SiO_2/Si substrates and their characterizations. The ultrathin layers of these materials have been characterized using non-destructive techniques including optical microscopy, AFM, and Raman spectroscopy. We report, for the first time, the 2D nature of GaS and GaSe isolated sheets from bulk materials using a scotch tape micromechanical cleavage technique.

2. Results and Discussion

Single-layer MoS_2 was prepared by the standard micromechanical cleavage procedures[2] from bulk MoS_2 crystal (purchased from SPI suppliers) on 50 nm, 300 nm, and 500 nm SiO_2/Si substrates. **Figure 2** shows the optical images of single-layer (marked with a red oval in optical image) and few-layer MoS_2 flakes deposited on a) 50 nm, d) 300 nm, and g)

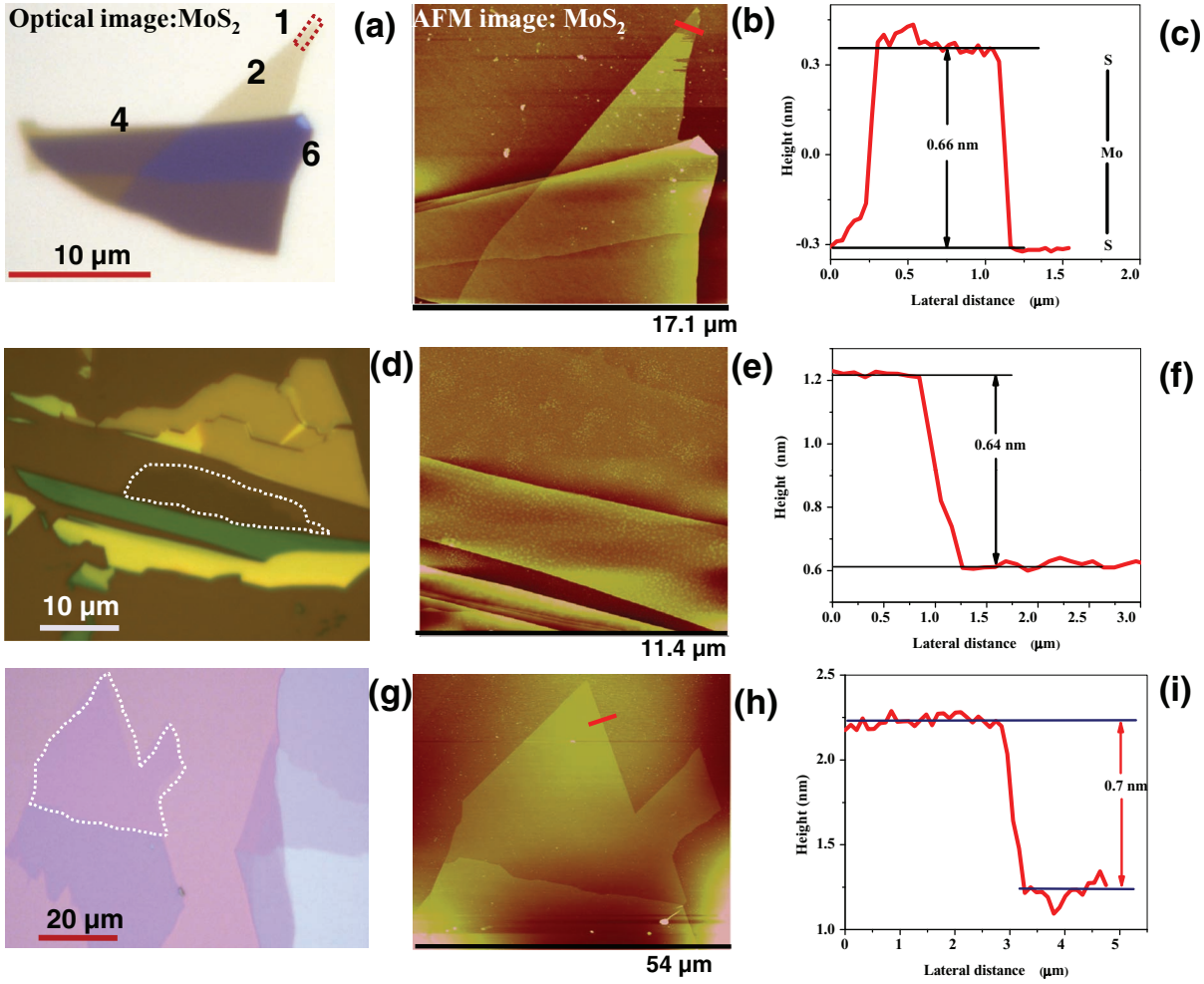

Figure 2. Optical images of single-layer (highlighted by a dashed line) and few layer MoS_2 flakes deposited on a) 50 nm (1, 2, 4, and 6 indicates the number of layers in the MoS_2 flake), d) 300 nm, and g) 500 nm SiO_2/Si substrate using a micromechanical cleavage method. AFM images of single-layer MoS_2 deposited on b) 50 nm, e) 300 nm, and h) 500 nm SiO_2/Si substrates. The corresponding AFM height profiles are shown in (c,f,i).

500 nm SiO_2/Si substrates. Figure 2b,e,h shows the corresponding AFM images of the MoS_2 single layer and few layers deposited on b) 50 nm, e) 300 nm, and h) 500 nm SiO_2/Si substrates. Figure 2c,f,i shows the corresponding AFM height profile. The AFM height profile shows single-layer MoS_2 has a thickness of 0.62 nm. **Figure 3**a shows the comparative Raman spectra of bulk and single-layer MoS_2. Figure 3b shows the Raman spectrum of MoS_2 thickness dependence of A^1_g and E^1_{2g} mode. Figure 3c show a Raman shift as function of MoS_2 layers. Raman spectrum of single-layer and multilayer MoS_2 clearly show the thickness dependence of in-plane (E^1_{2g}) and out-of-plane (A_{1g}) Raman modes along with both modes shifting away from each other in frequency with increasing thickness.

We observed an increasing intensity as well as a line width increase for both Raman modes as reported previously.[21] Figure 3d shows the Raman spectra of single-layer MoS_2 as a function of laser power. By analyzing the laser power variation data for single-layer MoS_2, the downshifting of both the E^1_{2g} and A_{1g} Raman modes was found and an increase in line width with increasing laser power was observed, as shown in Figure 3d. The laser power dependence of the A_{1g} and E^1_{2g} peak frequencies has been obtained by a Lorentzian line-fitting procedure and is shown in Figure 3e,f. An increase in laser power increases the local temperature, which reduces the stability of the excitons. This causes an excitation of electrons into the conduction band, until the excitons dissociate.

Figure 4 a,d,g are optical images of ultrathin and few-layer GaS deposited on a) 50 nm, d) 300 nm, and g) 500 nm SiO_2/Si. Figure 4b,e,f show corresponding AFM images and Figure 4c,f,i show corresponding height profiles marked in the AFM image of the GaS layer. Raman spectroscopy was also carried out on ultrathin and few layer GaS to find the relationship between the Raman mode shift and the GaS layer thickness. **Figure 5**a shows the comparative Raman spectra of bulk and ultrathin layer of GaS. Typically bulk GaS shows Raman modes E^1_{1g} (73.8 cm^{-1}), A^1_{1g} (187.93 cm^{-1}), E^1_{2g} (295.41 cm^{-1}), and A^2_{1g} (359.58 cm^{-1}). Figure 5b depicts the Raman spectra of GaS as function of layer thickness, calculated from AFM height profile. The frequencies shifts of the ultrathin layer GaS Raman modes at room temperature were found be E^1_{1g} (73.12 cm^{-1}), A^1_{1g} (185.53 cm^{-1}), E^1_{2g} (302.5 cm^{-1}), and A^2_{1g} (361.18 cm^{-1}). Figure 5c–e shows the dependence of Raman E^1_{2g}, A^1_{1g}, and A^2_{1g} modes as a function of layer thickness of GaS. The line width of the layered GaS phonons was studied systematically as a function

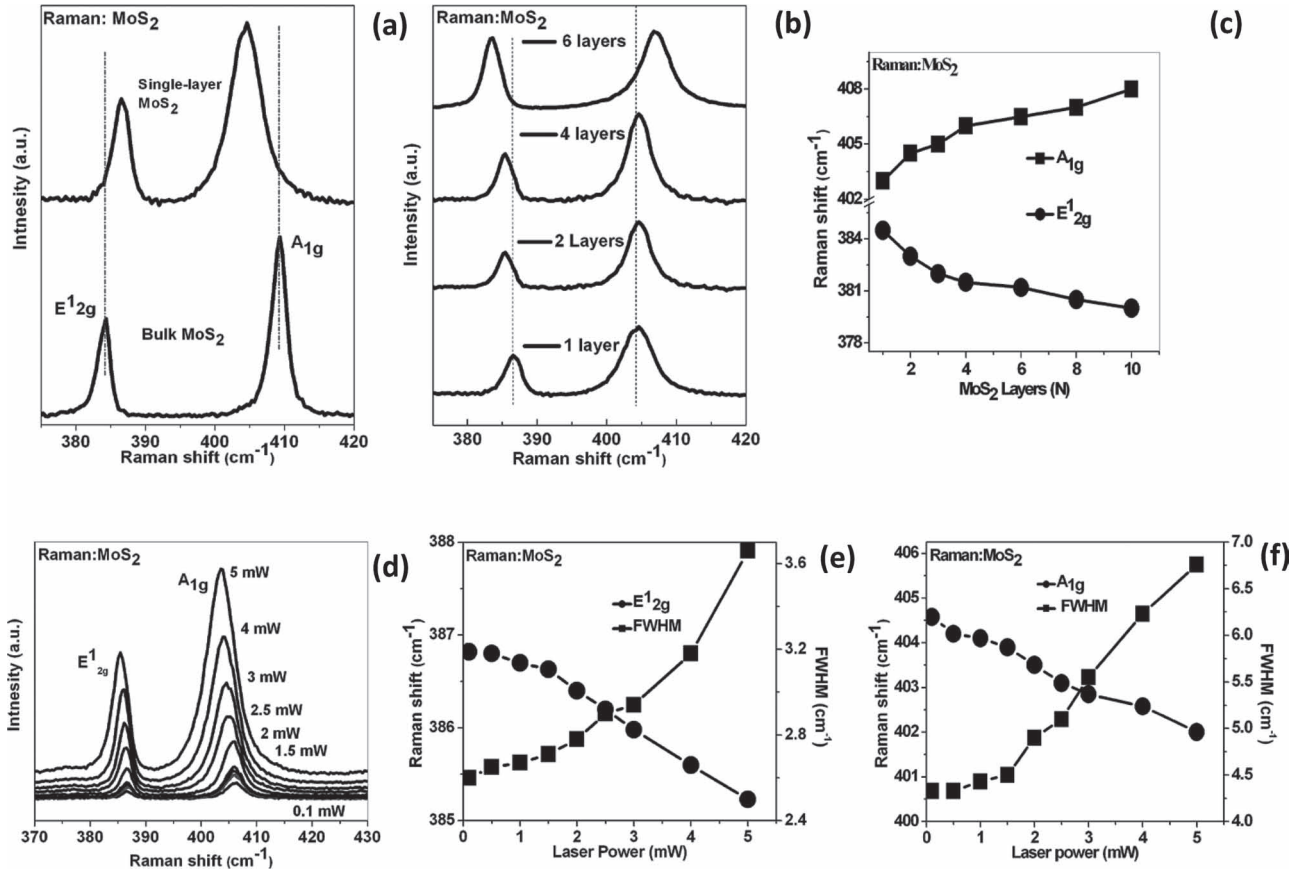

Figure 3. a) Comparative Raman spectroscopy of single-layer and bulk MoS_2, b) Raman spectra as a function of MoS_2 layer thickness variation with A_{1g} and E^1_{2g} modes, and c) Raman shift as function of MoS_2 layers. d) Raman spectroscopy of single-layer MoS_2 obtained by varying the laser power. From top to bottom, 5 mW, 4 mW, 3 mW, 2.5 mW, 2 mW, 1.5 mW, 1mW, 0.5 mW, 0.1 mW. Effect of laser power variation on the peak position and full width at half-maximum (FWHM) for e) A_{1g} mode and f) E^1_{2g} mode.

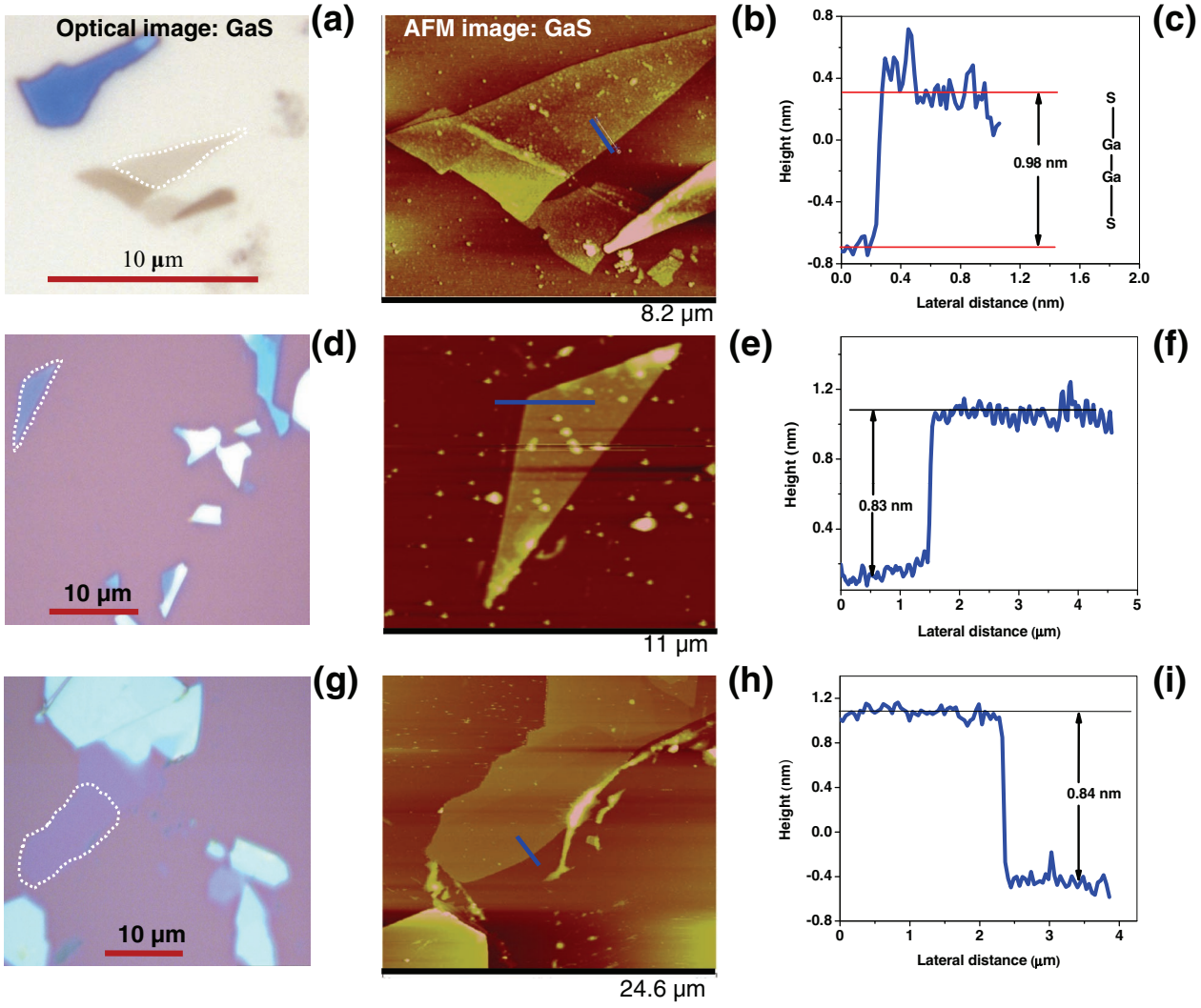

Figure 4. Optical images of ultrathin layer (highlighted by a dashed line) and few layers GaS flakes deposited on a) 50 nm, d) 300 nm, and g) 500 nm SiO_2/Si. AFM images of ultrathin GaS layer deposited on b) 50 nm, e) 300 nm, (and) 500 nm SiO_2/Si and corresponding AFM height profiles for c) 50 nm, f) 300 nm, and i) 500 nm SiO_2/Si.

of layer thickness and is also shown in Figure 5c–e on the right axis. The line widths of all Raman modes were found to increase as a function of decreasing layer thickness, as previously described for the temperature dependence of GaS layered crystal.[30] We have also studied the effect of laser power variation on GaS layers on A^1_{1g} and A^2_{1g} modes and the data are shown in Figure 5f.

Figure 6a,d,g shows optical images of ultrathin and multilayers of GaSe flakes deposited on a) 50 nm, d) 300 nm, and g) 500 nm SiO_2/Si. In Figure 6b,e,h we show the corresponding AFM images and Figure 6c,f,i shows corresponding AFM height profile of the GaSe layers. **Figure 7**a shows the Raman spectra of GaSe as a function of layer thickness (calculated from the AFM height profile). The Raman spectra of SiO_2/Si are also shown in Figure 7a for comparison. Figure 7b shows Raman spectra of a 1 nm thick layer GaSe sheet and a bulk GaSe crystal. Raman spectrum of bulk GaSe consists of three intense bands and one very weak band, which are characteristics of the GaSe single crystal. Raman spectrum of bulk GaSe crystal consists intense peaks for the A^1_{1g} mode (133 cm^{-1}), E^1_{2g} mode (211.9 cm^{-1}), and A^2_{1g} (306.8 cm^{-1}), in addition to one weak peak for the mode E^2_{1g} (250 cm^{-1}).[31–34] In an ultrathin layer of GaSe the Raman scattering signals from the A^1_{1g} mode and E^1_{2g} mode disappeared, the E^2_{1g} (256 cm^{-1}) mode become more intense and the mode A^2_{1g} (301 cm^{-1}) was observed to be shifted towards the lower wavelength side. The appearance of a more intense Raman E^2_{1g} mode was previously observed for Raman scattering of GaSe single crystals under heat and pressure treatment.[32] The intensities of the Raman modes are observed to decrease with decreasing layer thickness for both GaS and GaSe. The GaSe crystal changes its color gradually to dark brown on the 50 nm SiO_2, light green on the 300 nm SiO_2, and light purple on the 500 nm SiO_2 substrate. Figure 7c,d shows the effect of GaSe layers thickness on Raman c) A^2_{1g} and d) A^1_{1g} modes.

To quantify the contrast of MoS_2 on SiO_2 substrate, we calculated the optical contrast using Fresnel law, which was developed by Blake et. al.[4] for single-layer graphene. The reflected

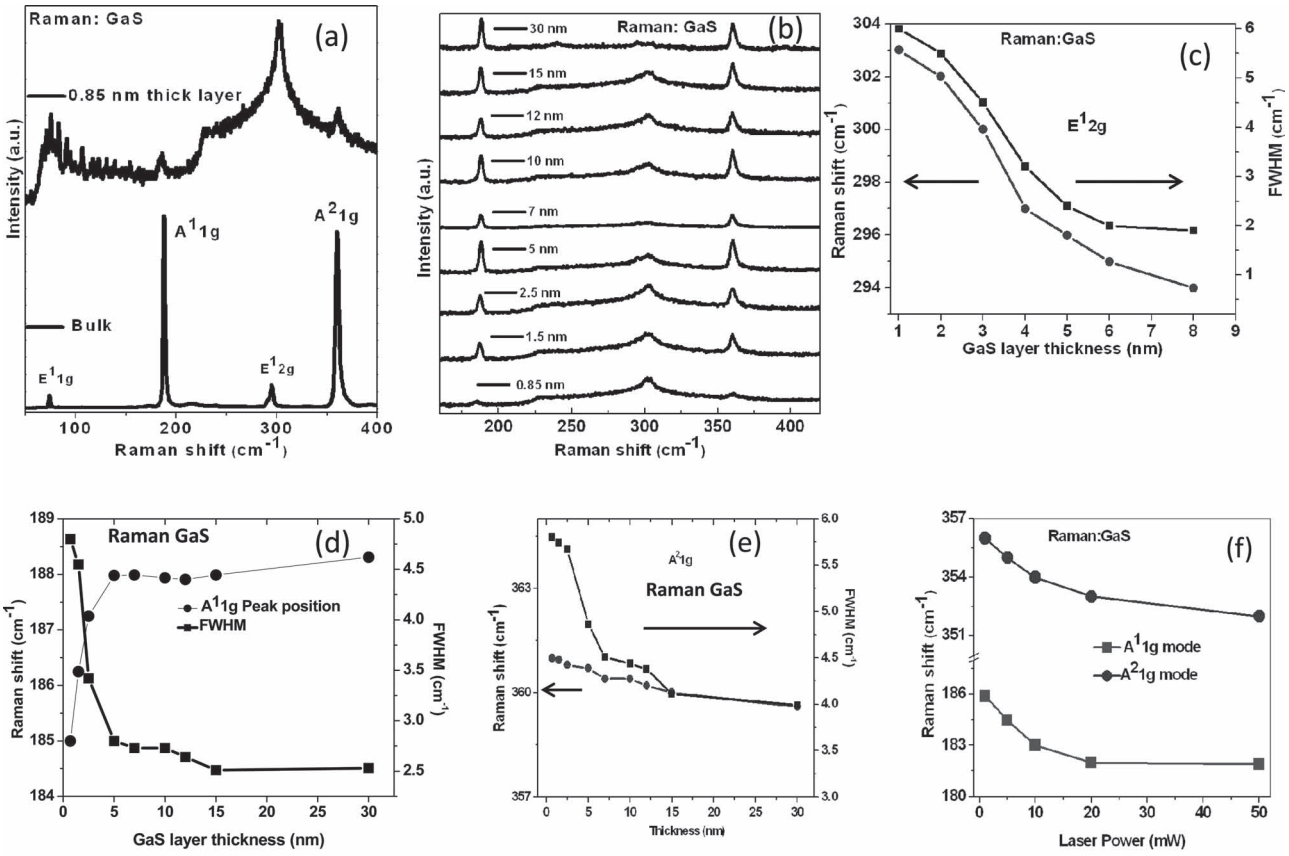

Figure 5. a) Raman spectra of bulk and ultrathin layer GaS and b) Raman spectra of GaS as a function of layer thickness. Effect of GaS layer thickness on c) E^1_{2g}, d) A^1_{1g}, and e) A^2_{1g} modes. f) The effect of laser power variation on the GaS A^1_{1g} and A^2_{1g} modes.

intensity for normal incidence of monochromatic light can be calculated by using the equation

$$I = |r_{01}e^{i(\Phi_1+\Phi_2)} + r_{12}e^{-i(\Phi_1-\Phi_2)} + r_{23}e^{-i(\Phi_1+\Phi_2)} + r_{01}r_{12}r_{23}e^{i(\Phi_1-\Phi_2)2}/e^{i(\Phi_1+\Phi_2)} + r_{01}r_{12}e^{-i(\Phi_1-\Phi_2)} + r_{01}r_{23}e^{-i(\Phi_1+\Phi_2)} + r_{12}r_{23}e^{i(\Phi_1-\Phi_2)}|^2 \quad (1)$$

where the subindices 0, 1, 2, and 3 refer to the media air, flake, SiO_2, and Si, respectively. $r_{ij} = (n_i - n_j)/(n_i + n_j)$ and $\phi_i = 2\pi n_i d_i/\lambda$ with n_i the complex refractive index, d_i the thickness of the medium i, and λ the wavelength. Therefore optical contrast of the flake can be defined as:

$$\text{Optical Contrast} = (I_{\text{flake}} - I_{\text{substrate}})/(I_{\text{flake}} + I_{\text{substrate}}) \quad (2)$$

I_{flake} can be directly calculated from Equation (1) and $I_{\text{substrate}}$ can be obtained by assuming that the medium 1 is air instead of a flake. The optical contrast of MoS_2 is calculated as an example to show the criteria of selection of SiO_2 thickness and the dependence of the layer number of MoS_2 thin films. The optical contrast of the MoS_2 flakes deposited on three different SiO_2/Si substrates with 50 nm, 300 nm, and 500 nm of SiO_2 were calculated as a function of their thickness at different illumination wavelengths. First, we plotted the contrast of the monolayer MoS_2 and bilayer MoS_2 as a function of the wavelength and the thickness of SiO_2 in **Figure 8**a,b, respectively.

Clearly, there are four characteristic bands with high positive contrast, which correspond to SiO_2 thickness of 50–100 nm, 175–250 nm, 300–375 nm, and 450–500 nm, implying that MoS_2 ultrathin films on such substrates should be visible for some spectral ranges of the visible light. To confirm these results, we synthesized the MoS_2 single-layer samples on 50 nm, 300 nm, and 500 nm SiO_2/Si substrates and the corresponding optical images are shown in Figure 2a,d,g, respectively. The contrast changes with the increase of layer number of MoS_2 were further simulated for the aforementioned SiO_2 thicknesses. **Figure 9**a,c,e shows the color plots corresponding to 50 nm, 300 nm, and 500 nm thick SiO_2, respectively. In order to determine the thickness with the optical contrast, the monotonic relationship between the film thickness and the contrast is critical. However, from Figure 8, though the contrast does correlate strongly to the illumination wavelength and the layer number, the contrast does not always increase with the layer number monotonically for specific wavelength and SiO_2 thickness.

Considering that the typical Bayer filter used in color cameras contains over 50% green elements, we plotted the contrast versus MoS_2 layer number at 500 nm wavelength, as shown in Figure 9b,d,f. Figure 8a,b shows the color plot of the contrast as a function of wavelength and SiO_2 thickness according to

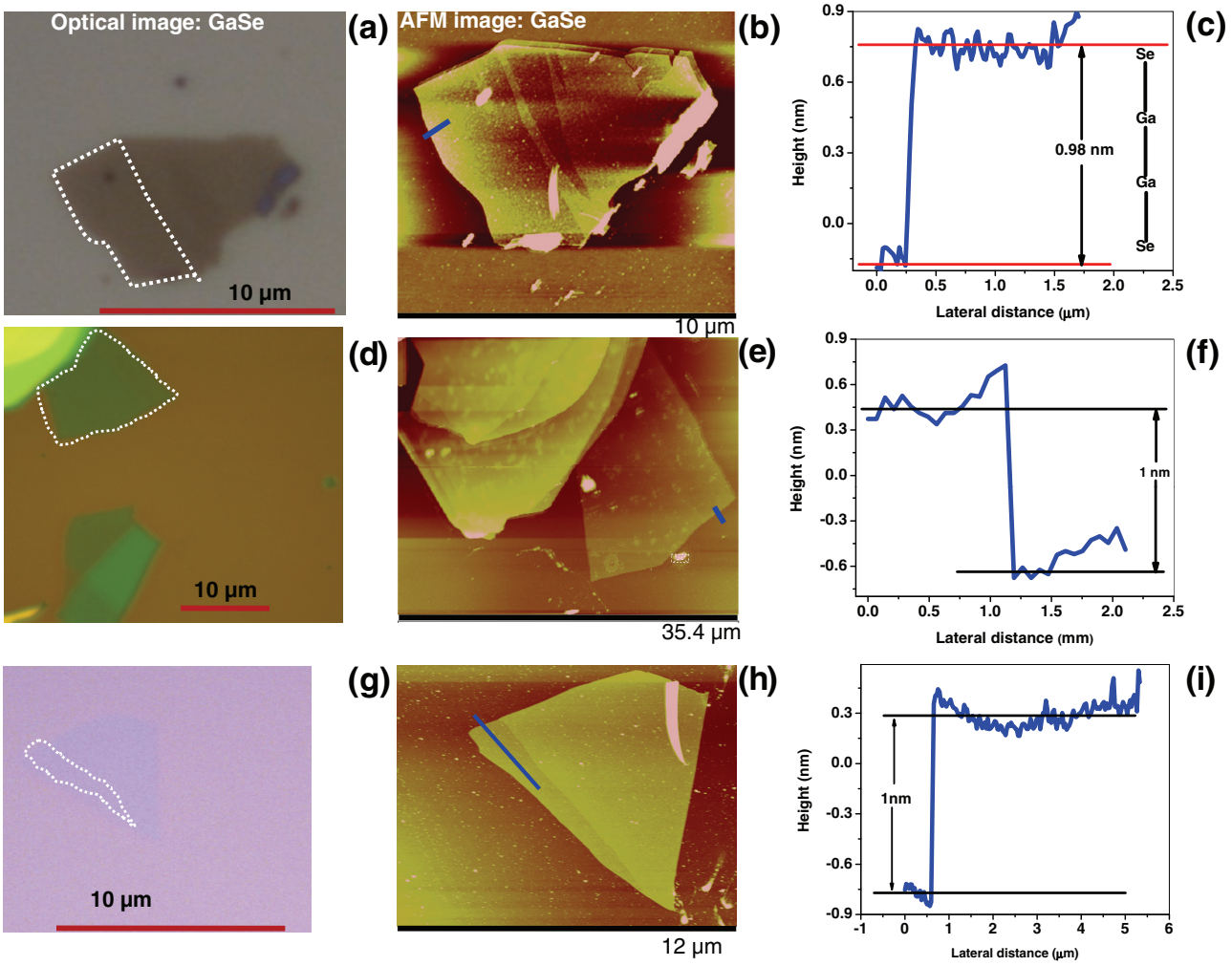

Figure 6. Optical images of ultrathin layer (highlighted by a dashed line) and few layers of GaSe flakes deposited on a) 50 nm, d) 300 nm, and g) 500 nm SiO_2/Si. AFM images of ultrathin GaSe layers deposited on b) 50 nm, e) 300 nm, and h) 500 nm. Corresponding AFM height profile for GaSe deposited on c) 50 nm, f) 300 nm, and i) 500 nm SiO_2/Si.

Equation (2). The color scale on the right shows the expected contrast for single-layer (Figure 8a) and bilayer (Figure 8b) MoS_2 sample. For a given layer thickness the contrast strongly depends on the illumination wavelength and, interestingly, thicker layers can yield lower contrast than thinner ones. The contrast does not monotonically increase as a function of the flake thickness and, in fact, can even decrease as the number of layers increases. Using the Fresnel law, we have measured the contrast versus the wavelength, the film thickness, and SiO_2 thickness. By applying the model for the refractive index values taken from the literature[35] we have calculated in the visible spectrum for MoS_2 with flakes composed by ≈10 layers down to monolayer. We are able to optimize the SiO_2 thickness, which allows for the explicit identification of ultrathin layer of MoS_2, GaS, and GaSe layered material. In this way, MoS_2 monolayers can be better identified if a SiO_2 thickness of either 55 or 220 nm is chosen, yielding a contrast 60% for 500 nm wavelength illumination.

Furthermore, we carried out Raman imaging of MoS_2, GaS, and GaSe layered materials to precisely determine the thickness and number of layers in the sample. **Figure 10**a shows the optical image of a MoS_2 sample deposited on the 300 nm thick SiO_2/Si substrate. The MoS_2 sheet contains one, three, five, and ≈96 layers, as predetermined by AFM (shown in Figure 10b). Figure 10c shows the Raman imaging of the MoS_2 sample. For comparison we have also shown the Raman spectra collected from single-layer and multilayer MoS_2 samples in Figure 10d. The differences between the MoS_2 samples with varying thicknesses are very noticeable. It can be clearly seen the broadening as well as peak position shift in both E^1_{2g} and A^1_g modes as function number of layers. This can be used to determine the number of layers present in the layered MoS_2 sample.

The advantage of Raman spectroscopy and imaging in determining the number of MoS_2 layers is that it does not depend on the substrate used. This is because the Raman spectrum is an intrinsic characteristic of a material. **Figure 11**a shows the optical image of GaS layered sample deposited on 500 nm thick SiO_2/Si substrate. The Figure 11b shows the corresponding AFM image of GaS layer sample while Figure 11c shows the

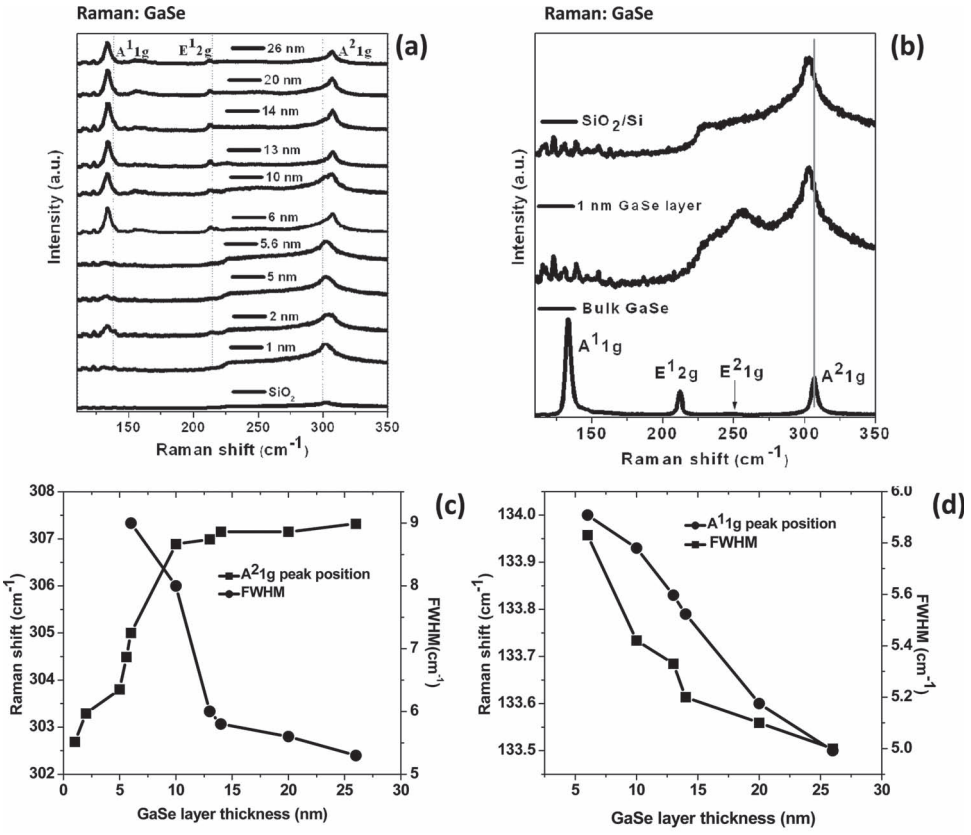

Figure 7. a) Raman spectroscopy of GaSe as a function of layer thickness. The Raman spectrum of the SiO_2/Si substrate is also shown for reference. b) Raman spectra of SiO_2/Si substrate, 1 nm thick GaSe layer and bulk GaSe. Effect of the layer thickness on the Raman c) A^2_{1g} and d) A^1_{1g} modes.

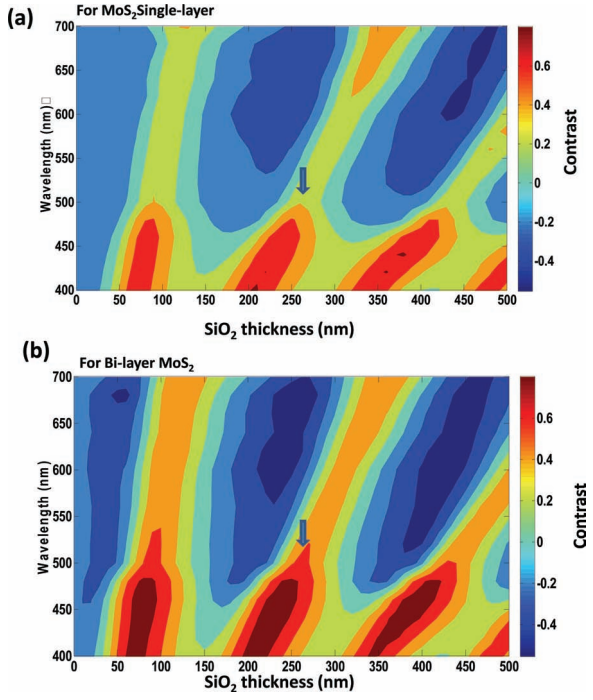

Figure 8. Color plot of calculated contrast as a function of incident light wavelength and SiO_2 layer thickness for a) single-layer MoS_2 and b) bilayer MoS_2 according to Equation (2). The color scale on the right shows the expected contrast. Arrow in (a,b) indicate the better contrast to identify the single-layer and bilayer MoS_2.

Raman imaging of a GaS sample. In Figure 11d we show the Raman spectra collected from a 1 nm thin-layer GaS sample as well from that of a 18 nm thick GaS layer sample. **Figure 12**a shows the optical image of GaSe layered sample deposited on 500 nm thick SiO_2/Si substrate. In Figure 12b we show the corresponding AFM image of the GaSe layer sample while Figure 12c shows the Raman imaging of GaSe layer sample. Figure 12d shows the Raman spectra collected from a 1 nm thin-layer GaSe sample as well from that of a 20 nm thick GaSe layer sample.

In summary, we have demonstrated the preparation and characterization of large size layered materials MoS_2, GaS, and GaSe using mechanical exfoliation on various thicknesses of SiO_2, followed by optical imaging, AFM, and Raman imaging. We also report the contrast characteristics of chalcogenide layers on SiO_2/Si substrates, which makes it is easier to determine the number of layers directly. We have calculated the contrast using Fresnel's equations and the simulations allow extraction of the contrast of monolayer and bilayer of chalcogenides such as MoS_2. An analytical expression for determining the number of layers is developed. From the contrast in the images, we demonstrate the effectiveness of this technique, which provides a fast, nondestructive, easy-to-use, accurate, and unambiguous method to identify the number of layers in the sample. We believe this collective contribution will assist researchers in further exploring these exciting classes of layered materials for scientific and technological pursuits.

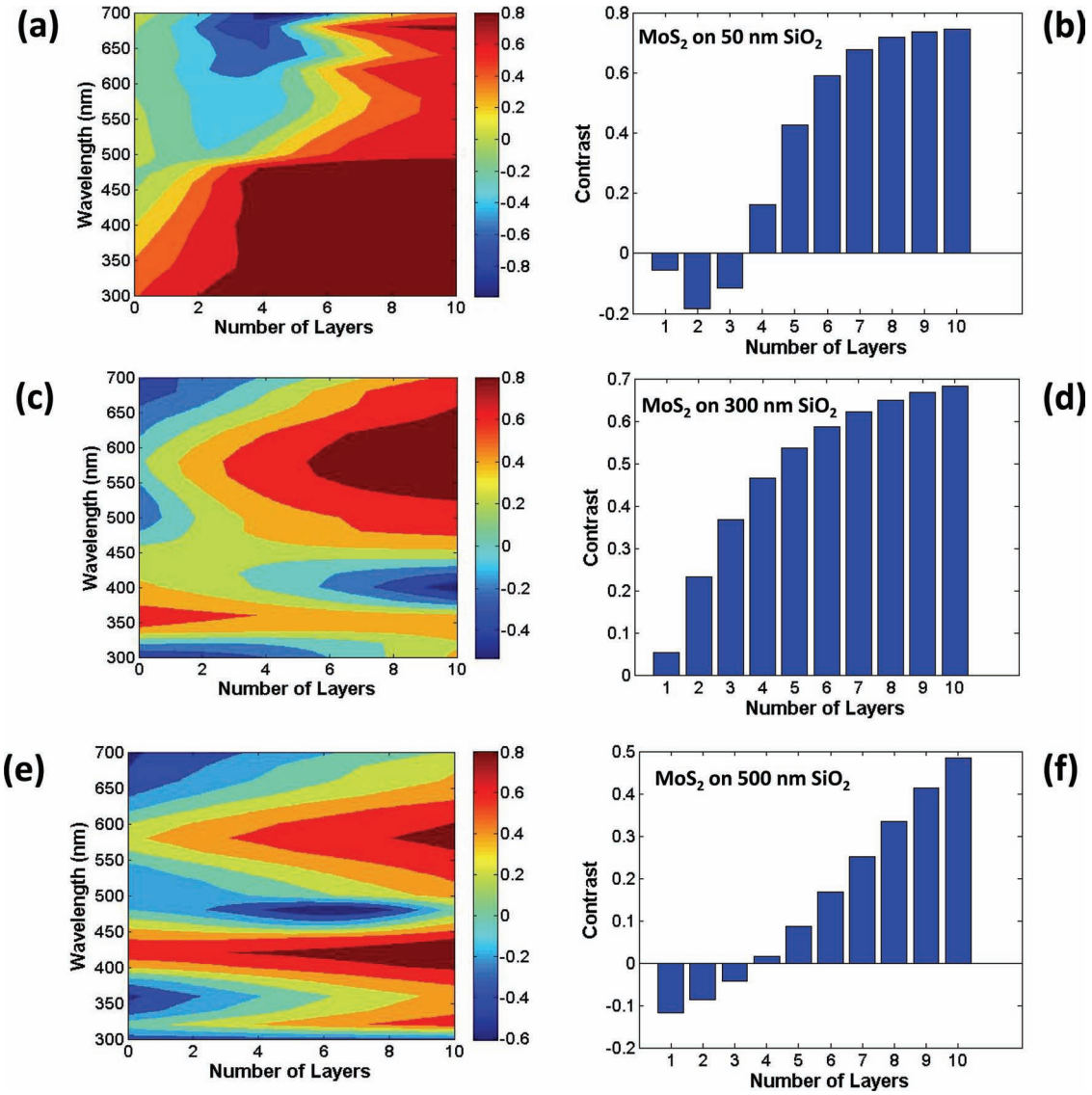

Figure 9. Color contrast plot of calculated contrast as a function of the number of layers of MoS_2 ultrathin films and the illumination wavelength for 50 nm (a,b), 300 nm (c,d), and 500 nm (e,f) thick SiO_2/Si substrates.

3. Conclusion

Ultrathin layers of MoS_2, GaS, and GaSe were prepared using the mechanical exfoliation technique, which is widely employed for the case of single-layer graphene on top of an SiO_2/Si wafer. Ultrathin flakes were identified using optical microscopy and further corroborated with complementary AFM imaging and Raman spectroscopy. The identification of atomically thin layers of GaS and GaSe is much more difficult than single-layer graphene as the former does not absorb visible light and, therefore, gives rise to contrast only because of changes in the optical path length. Notwithstanding these constraints, we show that the use of thinner SiO_2 and/or narrow optical filters, it is possible to optically observe even GaS and GaSe ultrathin layers. To verify the number of layers, we employed Raman spectroscopy along with AFM. Raman spectroscopy allows identification of ultrathin layers by a shift in the Raman peak position, change in the intensity, and a change in the line-broadening. The change in the Raman intensity can be used for further confirmation and for counting the number of layers in the samples. Further, the Raman intensity was observed to increase with decreasing layer thickness of MoS_2, while in case of GaS and GaSe the trend appears reversed. We have also calculated the expected contrast between the ultrathin layers for these materials deposited on 50 nm, 300 nm, and 500 nm SiO_2/Si. We believe that the provided analysis and the strategy for identifying ultrathin layers and few-layers of MoS_2, GaS, and GaSe should facilitate and accelerate further work on property/phenomena measurements by invoking rapid and non-invasive optical characterization to isolate specific layers for measurements.

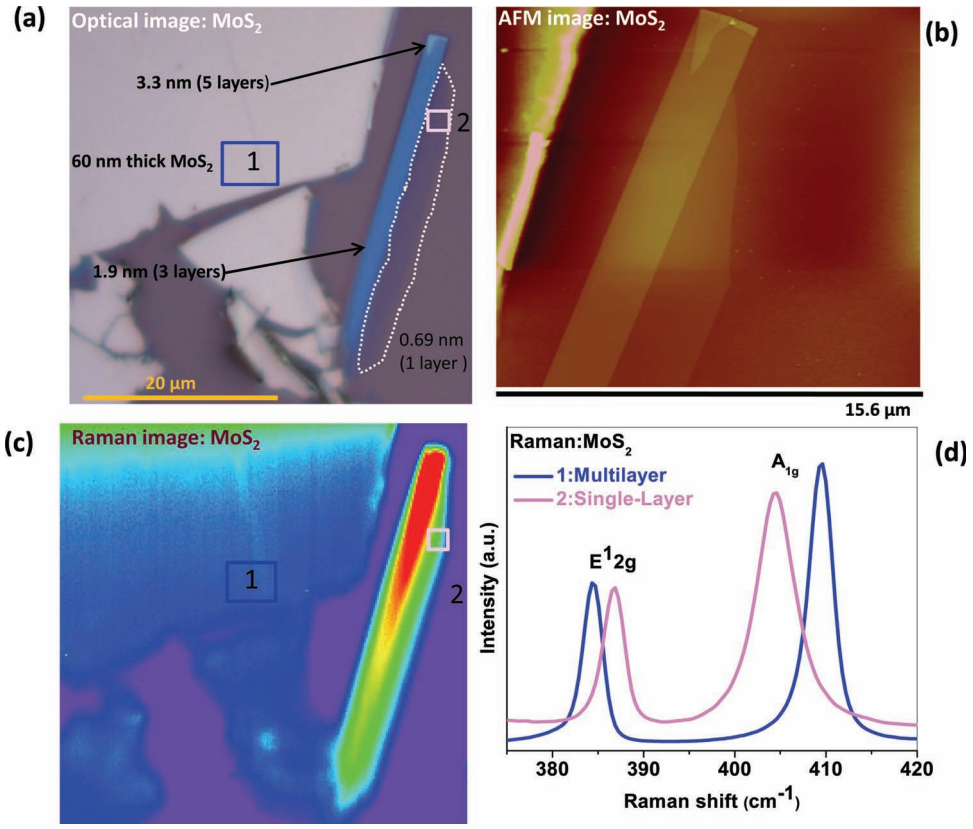

Figure 10. a) Optical image of single-layer MoS_2 sheet (highlighted by a dashed line) on a 300 nm SiO_2/Si substrate, b) corresponding AFM image of a single-layer MoS_2 sheet, and c) Raman image of single-layer MoS_2 sheet. d) Raman spectra of MoS_2 collected from the highlighted red square region 1 shown in the Raman image (multilayer MoS_2) and the blue square region 2 (single-layer MoS_2).

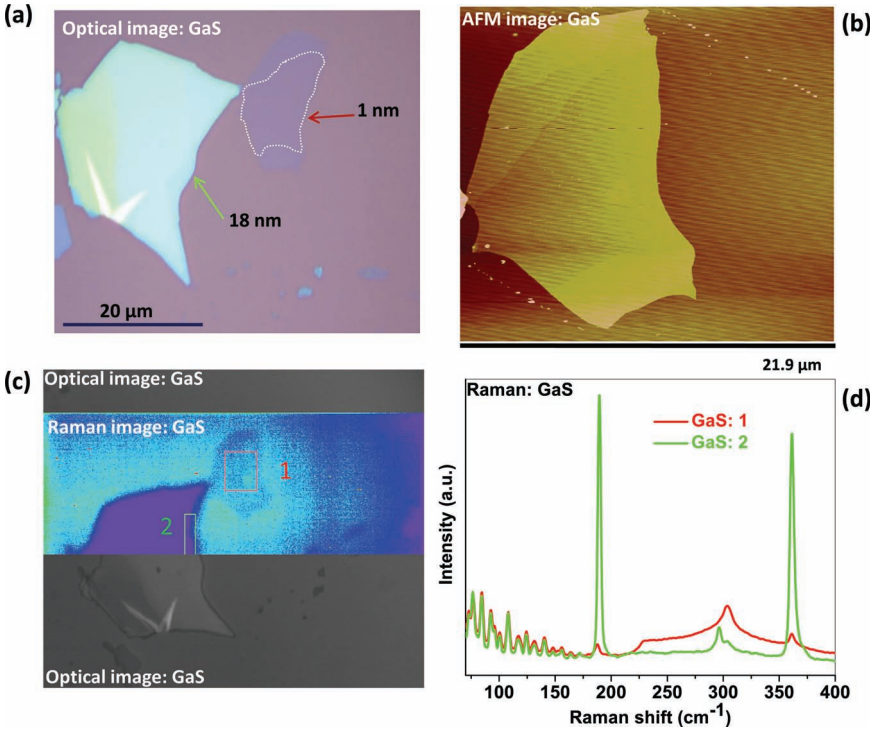

Figure 11. a) Optical image of ultrathin layer GaS sheets (highlighted by a dashed line) on a 500 nm SiO_2/Si substrate, b) corresponding AFM image of GaS sheet, and c) Raman image of ultrathin layer GaS sheet. d) Raman spectra of ultrathin layer GaS collected from region 1 (marked as a red colored square in the Raman image) and multilayer GaS marked as region 2 (green square in the Raman image).

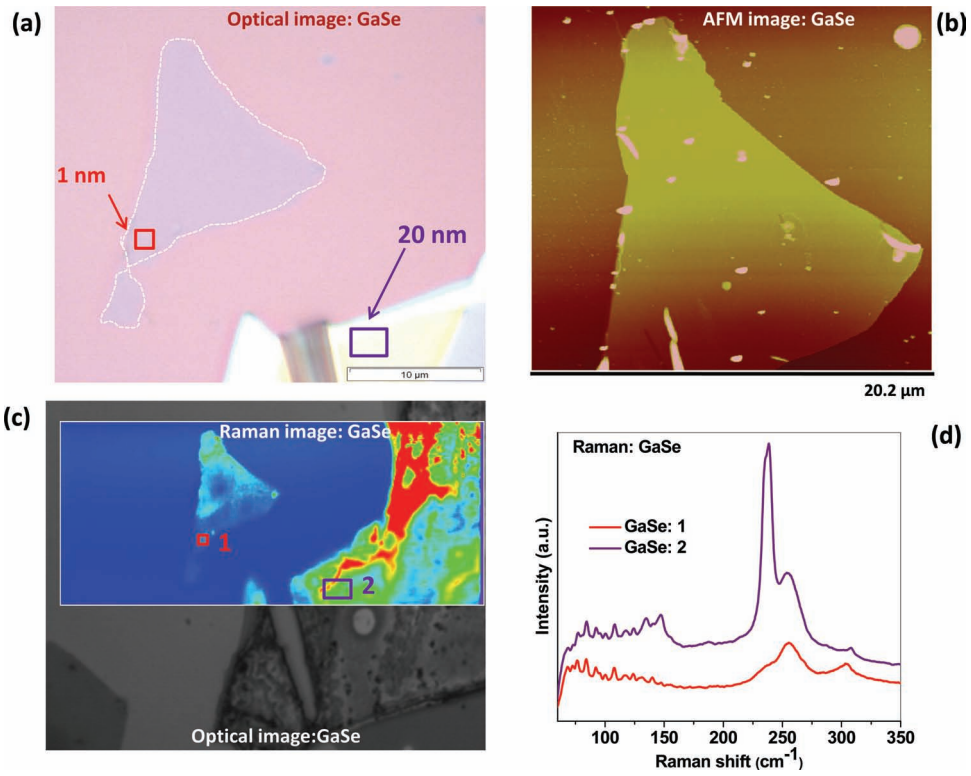

Figure 12. a) Optical image of ultrathin layer GaSe sheet (highlighted by a dashed line) on a 500 nm SiO_2/Si substrate, b) corresponding AFM image of GaSe sheet, and c) Raman image of an ultrathin layer GaSe sheet. d) Raman spectra of ultrathin layer GaSe collected from region 1 (highlighted as red colored square in the Raman image) and multilayer GaSe (highlighted as purple in the Raman image).

4. Experimental Methods

Ultrathin Layer Preparation: The SiO_2/Si substrates were thoroughly cleaned using a standard RCA cleaning method followed by boiling in acetone and isopropyl alcohol for 5 min. Finally, substrates were cleaned using an oxygen plasma for 5 min. Single-layer of MoS_2, GaS, and GaSe were deposited at room temperature in ambient conditions by standard mechanically exfoliating method using bulk materials onto cleaned SiO_2/Si substrates (with thicknesses of 50 nm, 300 nm, and 500 nm) in a manner similar to that previously established for single-layer graphene.[2] After deposition of thin samples, the thinnest flakes were identified by using optical microscopy. The exfoliated thinnest flakes had typical dimensions of tens of micrometers.

Optical Microscopy: An optical microscope was used to locate the sheets of MoS_2, GaS, and GaSe and the thickness was further confirmed using AFM and Raman spectoscopy. The optical microscopy images were acquired with an optical microscope (Nikon Eclipse ME600) imager M1m with white light illumination (100 W halogen lamp, HAL100) using a bright-field imaging mode and 100× objectives. In all cases, the Nikon Eclipse ME600 was used to record the optical images using color-view mode with a soft imaging system. For each filter, 100 frames were averaged to produce the final image. Exposure times varied in the range of 10 to 300 ms depending on the filter.

Atomic Force Microscopy: AFM tapping mode images were recorded using an ICON system (Bruker, Santa Barbara Ca). To obtain a more accurate reading of the AFM height profile, the as synthesized ultrathin layer sample was annealed at 400 °C in Ar + H_2 atmosphere for 2 h.

Raman Spectroscopy: Raman spectroscopy is a potential candidate for non-destructive and quick inspection of the thickness of graphene and graphene-like layered materials. Raman spectra were collected in back scattering geometry using the system (a Nano-photon Raman-11). In Raman spectroscopy, the 532 nm line of an Ar ion laser was used as the excitation source with laser power of ≈1mw. The laser beam was focused onto the as-synthesized, ultrathin, layered samples by using a 100× microscope objective lens and the scattered light was collected in the backscattering geometry. The collected scattered light was dispersed by spectrometer grating of 2400 mm and was detected with an electrically cooled charge-coupled detector (CCD) (–70° C). The spatial resolution was less than 0.8 μm and the spectral resolution was 0.39 cm^{-1} with a peak position accuracy 0.1 cm^{-1}.

Raman Imaging: The Raman spectra and imaging of the layered materials were recorded with a Nanophoton Raman 11 system a double-frequency Nd:YAG laser (532 nm) as the excitation source, with grating of 2400 mm^{-1} with: total exposure time (per line) = 30 s, readout speed = 2 MHz, gain = high, readout port = low noise, CCD temperature = –70 °C, optical line shaping mode, objective lens = LU Plan Fluor ×100/NA (numerical aperture) 0.9, measurement mode = XY-LAMBDA. The laser power at the sample was below 1 mW to avoid laser-induced heating. All spectra were recorded under the same experimental conditions.

Calculations of the Optical Contrast: The reflectance of the incident light was calculated for normal incidence of the objective lens taking into account interference and multiple reflections. The difference in reflectance was calculated based on bare SiO_2 substrate and substrate with MoS_2 thin films.

Supporting Information

Supporting Information is available from the Wiley Online Library or from the author.

Acknowledgements

The research was primarily supported by an Indo-US Science & Technology Forum (IUSSTF) grant between JNCASR (India) and Northwestern University (USA). Partial support by NSF-MRSEC and NSF-NSEC programs at NU is gratefully acknowledged. The research made use of the NU*ANCE* Center and BIF facilities at Northwestern University. D.J.L. would like to thank the Indo-US Science & Technology Forum (IUSSTF) for a postdoctoral fellowship. This article was amended on May 9, 2012. The presentation of the author's names was incorrect in the version originally publised online.

Received: November 24, 2011
Published online: February 16, 2012

[1] K. S. Novoselov, D. Jiang, F. Schedin, T. J. Booth, V. V. Khotkevich, S. V. Morozov, A. K. Geim, *Proc. Natl. Acad. Sci. USA* **2005**, *102*, 10451.
[2] K. S. Novoselov, A. K. Geim, S. V. Morozov, D. Jiang, Y. Zhang, S. V. Dubonos, I. V. Grigorieva, A. A. Firsov, *Science* **2004**, *306*, 666.
[3] K. S Novoselov, A. K. Geim, S. V. Morozov, D. Jiang, M. I. Katsnelson, I. V. Grigorieva, S. V. Dubonos, A. A. Firsov, *Nature* **2005**, *438*, 197.
[4] P. Blake, E. W. Hill, A. H. Castro Neto, K. S. Novoselov, D. Jiang, R. Yang, T. J. Booth, A. K. Geim, *Appl. Phys. Lett.* **2007**, *91*, 063124.
[5] Z. H. Ni, H. M. Wang, J. Kasim, H. M. Fan, T. Yu, Y. H. Wu, Y. P. Feng, Z. X. Shen, *Nano Lett.* **2007**, *7*, 2758.
[6] B. Radisavljevic, A. Radenovic, J. Brivio1, V. Giacometti, A. Kis, *Nat. Nanotechnol.* **2011**, *6*, 147.
[7] M. M. Benameur, B. Radisavljevic, J. S. Héron, S. Sahoo, H. Berger, A. Kis, *Nanotechnology.* **2011**, *22*, 125706.
[8] H. S. S. R. Matte, A. Gomathi, A. K. Manna, D. J. Late, R. Datta, S. K. Pati, C. N. R. Rao, *Angew. Chem. Int. Ed.* **2010**, *49*, 4059.
[9] C. Altavilla, M. Sarno, P. Ciambelli, *Chem. Mater.* **2011**, *23*, 3879.
[10] Y. Yoon, K. Ganapathi, S. Salahuddin, *Nano Lett.* **2011**, *11*, 3768.
[11] A. Ayari, E. Cobas, O. Ogundadegbe, M. S. Fuhrer, *J. Appl. Phys.* **2007**, *101*, 014507.
[12] C. Lee, Q. Li, W. Kalb, X. Liu, H. Berger, R. W. Carpick, J. Hone, *Science* **2010**, *328*, 76.
[13] N. E. Staley, J. Wu, P. Eklund, Y. Liu, L. Li, Z. Xu, *Phys. Rev. B* **2009**, *80*, 184505.
[14] A. Castellanos-Gomez, N. Agraït, G. Rubio-Bollinger, *Appl. Phys. Lett.* **2010**, *96*, 213116.
[15] R. V. Gorbachev, I. Riaz, R. R. Nair, R. Jalil, L. Britnell, B. D. Belle, E. W. Hill, K. S. Novoselov, K. Watanabe, T. Taniguchi, A. K. Geim, P. Blake, *Small* **2011**, *7*, 465.
[16] C. Berger, Z. Song, T. Li, X. Li, A. Y. Ogbazghi, R. Feng, Z. Dai, A. N. Marchenkov, E. H. Conrad, P. N. First, W. A. de Heer, *J. Phys. Chem. B* **2004**, *108*, 19912.
[17] R. Rosei, S. Modesti, F. Sette, C. Quaresima, A. Savoia, P. Perfetti, *Phys. Rev. B* **1984**, *29*, 3416.
[18] J. N. Coleman, M. Lotya, A. O'Neill, S. D. Bergin, P. J. King, U. Khan, K. Young, A. Gaucher, S. De, R. J. Smith, I. V. Shvets, S. K. Arora, G. Stanton, H. Kim, K. Lee, G. T. Kim, G. S. Duesberg, T. Hallam, J. J. Boland, J. J. Wang, J. F. Donegan, J. C. Grunlan, G. Moriarty, A. Shmeliov, R. J. Nicholls, J. M. Perkins, E. M. Grieveson, K. Theuwissen, D. W. McComb, P. D. Nellist, V. Nicolosi, *Science* **2011**, *331*, 568.
[19] A. Geim, *Science* **2009**, *324*, 1530.
[20] A. Splendiani, L. Sun, Y. Zhang, T. Li, J. Kim, C. Chim, G. Galli, F. Wang, *Nano Lett.* **2010**, *10*, 1271.
[21] C. Lee, H. Yan, L. E. Brus, T. F. Heinz, J. Hone, S. Ryu, *ACS Nano* **2010**, *4*, 2695.
[22] F. Levy, *Intercalated Layer Materials*, D. Ridel Publishing Company, Holland **1979**, p. 1–307.
[23] R. M. A. Lieth, *Preparation and Crystal Growth of Materials with Layered Structures*, D. Reidel Publishing Company, Dordrech, Holland, **1977**, p. 225–254.
[24] K. F. Mak, C. Lee, J. Hone, J. Shan, T. F. Heinz, *Phys. Rev. Lett.* **2010**, *105*, 136805.
[25] G. Shen, D. Chen, P. Chen, C. Zhou, *ACS Nano* **2009**, *3*, 1115.
[26] J. Q. Hua, Y. Bando, J. H. Zhan, Z. W. Liu, D. Golberg, *Appl. Phys. Lett.* **2005**, *87*, 153112.
[27] T. Kohler, T. Frauenheim, Z. Hajnal, G. Seifert, *Phys. Rev. B* **2004**, *69*, 193403.
[28] U. K. Gautam, S. R. C. Vivekchand, A. Govindaraj, C. N. R. Rao, *Chem. Commun.* **2005**, 3995.
[29] H. Peng, S. Meister, C. K. Chan, X. F. Zhang, Y. Cui, *Nano Lett.* **2007**, *7*, 199.
[30] N. M. Gasanly, A. Aydinli, H. Özkan, C. Kocaba, *Solid State Commun.* **2000**, *116*, 147.
[31] O. A. Balitskii, V. P. Savchyn, V. O. Yukhymchuk, *Semicond. Sci. Technol.* **2002**, *17*, L1-L4.
[32] A. M. Kulibekov, H. P. Olijnyk, A. P. Jephcoat, Z. Y. Salaeva, S. Onari, K. R. Allakhverdiev, *Phys. Status Solidi B* **2003**, *235*, 517.
[33] T. J. Wieting, J. L. Verble, *Phy. Rev. B* **1972**, *5*, 1473.
[34] T. D. Ibragimov, G. G. Kurbanova, V. S. Gorelik, *Phys. Status Solidi B* **1989**, *155*, 113.
[35] A. R. Beal, H. P. Hughes, *J. Phys. C: Solid State Phys.* **1979**, *12*, 881.